

CHALMERS
UNIVERSITY OF TECHNOLOGY

V-band (47-51 GHz) Triangular Lattice Dual-polarized Patch Unit Cell for SATCOM Phased Arrays

Downloaded from: https://research.chalmers.se, 2026-11-27 10:17 UTC

Citation for the original published paper (version of record):
Pavlidis, T., Schäfer, T., Svensson, T. et al (2026). V-band (47-51 GHz) Triangular Lattice Dual-polarized Patch Unit Cell for SATCOM Phased Arrays. IEEE International Symposium on Phased Array Systems and Technology

N.B. When citing this work, cite the original published paper.

© 2026 IEEE. Personal use of this material is permitted. Permission from IEEE must be obtained for all other uses, in any current or future media, including reprinting/republishing this material for advertising or promotional purposes, or reuse of any copyrighted component of this work in other works.

(article starts on next page)

V-band (47-51 GHz) Triangular Lattice Dual-polarized Patch Unit Cell for SATCOM Phased Arrays

Theodoros Pavlidis
Dept. of Electrical Engineering
Chalmers University of Technology
Gothenburg, Sweden
pavlidis@chalmers.se

Thomas Schäfer
Satcube AB
Gothenburg, Sweden
thomas.schafer@satcube.com

Tommy Svensson
Dept. of Electrical Engineering
Chalmers University of Technology
Gothenburg, Sweden
tommy.svensson@chalmers.se

Ahmed A. Kishk
Dept. of Electrical and Computer Engineering
Concordia University
Montreal, Canada
ahmed.kishk.antenna@gmail.com

Marianna V. Ivashina
Dept. of Electrical Engineering
Chalmers University of Technology
Gothenburg, Sweden
marianna.ivashina@chalmers.se

***Abstract*—A dual-polarized phased array antenna (PAA) unit cell (UC) in a triangular lattice for V-band (47.2–50.2 GHz, 50.4–51.4 GHz) low Earth orbit (LEO) satellite communication user terminals is presented. It addresses the necessity to enlarge the UC footprint at high frequencies while maintaining wide-scan performance ($\theta_s \leq 60^\circ$) under stringent printed circuit board (PCB) design rules. In contrast, solutions that are based on rectangular lattices compromise between wide scan range or enlarged UC footprint. At the same time, other triangular lattice arrays are either constrained by fabrication limitations that hinder scaling to beyond Ka-band frequencies, or are single-polarized. In an infinite array, we have achieved 2-D scanning in the principal planes up to $\theta_s \leq 60^\circ$ over a 6.85% bandwidth (47.2–50.55 GHz) with Active VSWR < 3 and a realized gain drop of less than 6 dB relative to the theoretical maximum for broadside scan. To the best of the authors' knowledge, this is the highest-frequency dual-polarized array in a triangular lattice proposed for implementation in PCB technology.**

***Index Terms*—V-band, microstrip antenna arrays, phased arrays, satellite communications, triangular lattice.**

I. Introduction

Satellite communications (SATCOM) are considered a promising solution for achieving ubiquitous connectivity. Low Earth orbit (LEO) SATCOM in particular have attracted interest due to the lower latency and reduced free-space path loss [1], [2]. To connect to LEO satellites, user terminals operating in the SATCOM Ku-band [Fig. 1] and beyond typically use high-gain beamsteering antennas [1]. While most research efforts have concentrated in the Ku-, K-, and Ka-bands, several pioneering works have recently focused on the SATCOM Q- and V-bands [3]–[12].

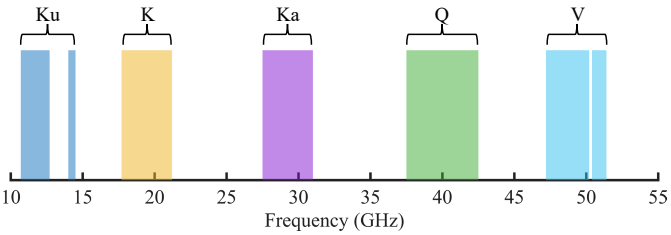

Fig. 1. Operating frequency bands of reported SATCOM terminals operating in the Ku- [15], K- [16], Ka- [17], and Q-/V- [3] bands.

For LEO SATCOM, an active planar phased array antenna (PAA) is a popular solution owing to its low profile, lack of moving parts, and rapid beamsteering. However, the small element spacing required for grating-lobe free scanning ($\sim \lambda_{\text{high}}/2 = 2.91$ mm at the highest operating frequency 51.4 GHz) restricts antenna-beamforming integrated circuit (BFIC) integration due to routing, assembly and thermal challenges. These challenges are exacerbated in dual-polarized arrays, where the number of BFIC channels is doubled. Dual polarization is, however, often demanded for SATCOM applications, since a dual-polarized phased array can generate switchable circular polarization [13], [14].

Dual-polarized PAAs beyond the Ka-band are mostly implemented in rectangular lattices (RELs) [12], [18]–[20]. RELs are characterized by adjacent elements arranged in perpendicular rows and columns, simplifying the co-location of dual orthogonal polarizations. To increase PAA unit cell (UC) footprint, the rectangular-lattice PAAs in [19], [20] have element spacings $> \lambda_{\text{high}}/2$. As a consequence, their scan

This work was supported in part by the Swedish Research Council (VR) through the 6G-NTN-E Research Environment under Grant 2024-06645. This work was also funded by the European Union, under ANTERRA 101072363 HORIZON-MSCA-2021-DN-01. Views and opinions expressed are however those of the author(s) only and do not necessarily reflect those of the European Union. Neither the European Union nor the granting authority can be held responsible for them.

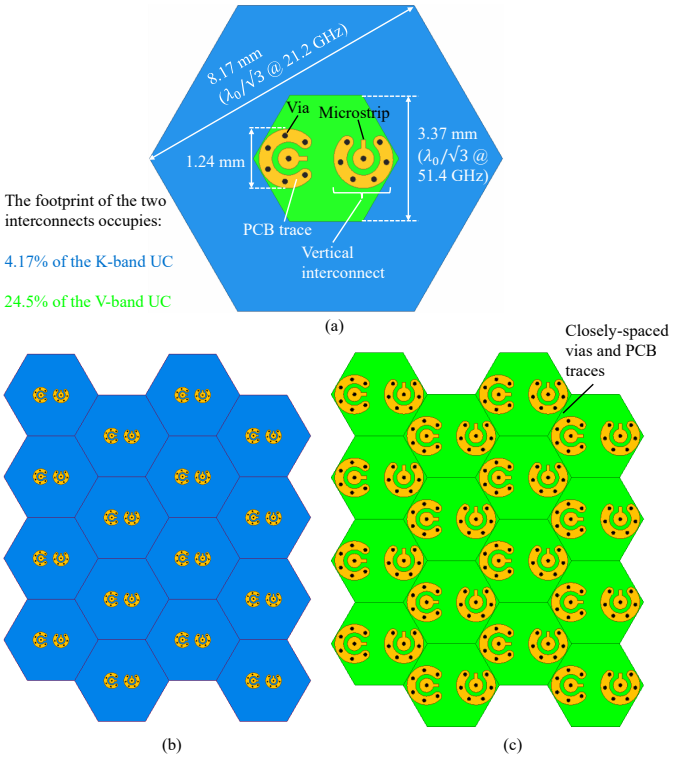

Fig. 2. Comparison of footprint constraints for the same vertical interconnects of two PAAs operating in the K- and V-band. (a) Two co-located UCs with vertical interconnects, (b) 16-element K-band sub-array with interconnects, and (c) 16-element V-band sub-array with interconnects. The interconnect footprint is identical to the interconnects used in this work, however, the interconnect placement differs.

range is limited to $\pm 55°$ or less. An alternative for increasing UC footprint while maintaining a $\pm 60°$ scan range is to use a triangular lattice (TL) [21]. It is well known that the equilateral TL enables a grating-lobe-free conical scan sector with an element footprint that is $2/\sqrt{3}$ (approximately 15.5%) larger than a REL [22]. While the TL has been commonly exploited in dual-polarized PAAs up to the SATCOM K-/Ka-bands [13], [16], [23]–[25], it is rarely reported at higher frequencies. One such array [26] is based in the planar ultrawideband modular (PUMA) topology and operates up to $f_{high} = 40$ GHz. To the best of the authors' knowledge, the patch PAA in [10] is the dual-polarized TL array with the highest reported $f_{high} = 42$ GHz. Unfortunately, using a TL for dual-polarized PAs at higher frequencies is constrained by several factors:

1) As wavelength decreases, PAA features become physically smaller, yet the design rule limitations (for example, minimum conductor width) remain fixed. An example of constraints introduced by the fixed design rules with regards to vertical interconnect integration is shown in Fig. 2. The physically smaller PAA features also complicate the usage of some fabrication and assembly techniques employed in lower frequencies, for example ground plane-radiator assembly with screws [27], [28], vertical interconnects with spring-like contacts [26], and PCB-integrated metal cavities [29].

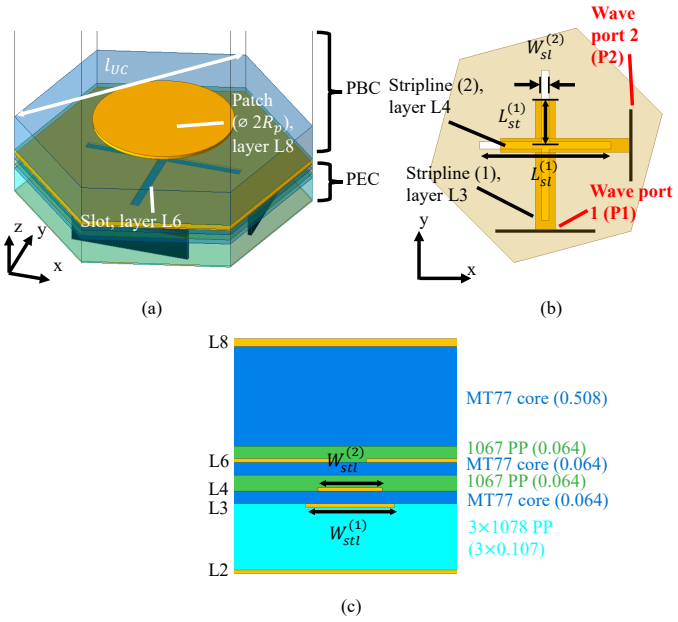

Fig. 3. Initial UC without vertical interconnects. (a) 3-D view with semi-transparent dielectric layers, (b) L3-L6 layers with semi-transparent L6 layer, and (c) PCB cross-section. $l_{UC} = 3.37$, $R_p = 0.93$, $L_{sl}^{(1)} = 2.11$, $L_{sl}^{(2)} = 2.41$, $W_{sl}^{(1)} = W_{sl}^{(2)} = 0.12$, $L_{st}^{(1)} = L_{st}^{(2)} = 0.71$, $W_{stl}^{(1)} = 0.32$, $W_{stl}^{(2)} = 0.23$. Units: millimeters. The superscripts (1) and (2) refer to dimensions corresponding to port 1 and port 2, respectively.

2) The inter-element mutual couplings differ in RELs and TLs, resulting in different scan impedance and radiation performance.
3) Adjacent elements are not arranged in perpendicular rows and columns, often making the co-location of two orthogonal polarizations non-trivial.

These factors combined complicate scaling of existing dual-polarized arrays in TLs to higher frequencies, make conversion of beyond Ka-band dual-polarized arrays from RELs [19], [20] to TLs difficult, and have so far limited most beyond Ka-band arrays in TLs to a single polarization [30]–[33].

The present work addresses this knowledge gap by proposing a dual-polarized cross-slot fed patch radiator in a TL for V-band SATCOM operation. The radiator and its feed lines, including the vertical interconnects necessary to ultimately connect the antenna to BFICs, are realizable using PCB technology.

The rest of the paper is organized as follows: Sec. II presents the UC design and investigates its performance in an infinite array environment. In Sec. III, conclusions are drawn.

II. Unit Cell Design

To ensure the manufacturability of the antenna using PCB technology, we have enforced the following design rules: 1) minimum conductor trace and conductor gap widths of 0.1 mm, 2) minimum via diameter of 0.15 mm, 3) minimum via annular ring of 0.1 mm, and 4) minimum via edge-to-via edge gap of 0.3 mm. These design rules are similar to those reported

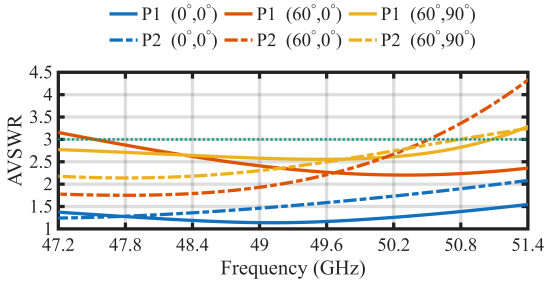

Fig. 4. Simulated port 1 and port 2 AVSWR of the UC without interconnects for (θ_s, ϕ_s) scan angle in a 2-D infinite array. The dotted line marks the AVSWR $= 3$ requirement.

for other beyond Ka-band antennas that are PCB-based [34]–[36].

An initial PAA UC without the interconnects is designed for broadside matching. This UC is depicted in Fig. 3. As shown in Fig. 3(a), the UC radiator consists of a patch placed on conductor layer L8 that is excited by a cross-slot etched on the ground plane on layer L6. This cross-slot is fed by two striplines, located on L3 and L4 [Fig. 3(b)]. The striplines feature an additional ground plane on layer L2 to prevent back radiation. In total, an 8-layer PCB utilizing Astra MT77 cores and prepregs (PPs) of standard thickness is used (see Fig. 3(c)). The presence of two ground planes on L2 and L6 raises the possibility of excitation of parallel-plate-waveguide (PPW) modes between them which can result in scan blindness. To prevent scan blindness, a PEC boundary condition surrounds the L2-L6 layers, as shown in Fig. 3(a). This boundary condition will later be replaced by vias. To simulate an infinite array in Ansys HFSS, periodic boundary conditions (PBCs) are applied in the UC sidewalls on L6 and above, while a Floquet port terminates the space above the aperture. Based on previous studies [37], we account for surface roughness using the Huray model, assuming copper conductivity with a nodule radius of 0.7 μm and a surface ratio of 3.8. The lattice is equilateral triangular.

The active VSWR (AVSWR) over frequency of this UC is illustrated in Fig. 4. Over 2.95 GHz (47.55-50.5 GHz), AVSWR remains below 3 for both UC ports when scanning at $0° \leq \theta_s \leq 60°$ in the principal (E-/H-) planes.

Since the scan bandwidth (for 60° E-/H-plane scanning) of the UC without the vertical interconnects spans most of the SATCOM V-band, at this stage, two vertical microstrip-to-stripline coaxial interconnects were designed separately from the antenna (with their transmission lines terminated to 50 Ω ports) and taking into account the PCB design rules. The interconnect geometry is depicted in Fig. 5(a). As shown in Fig. 5(a), six L1-L6 ground vias surround an L1-L4 signal via that connects the striplines on L3 and L4 to microstrip lines on L1. An L1-L4 signal via is used to shorten (for the port 1 interconnect) or eliminate (for the port 2 interconnect) the via stub extending beyond the via-stripline connection, lessening the effect of parasitic reactances on the interconnect return loss (RL) [38]. Similar to [34], [39], an L6 opening reduces

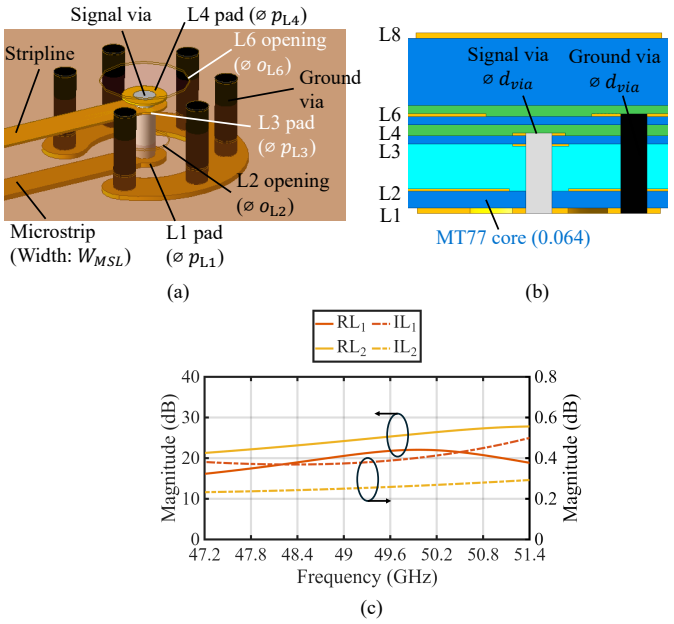

Fig. 5. Vertical interconnects. (a) Geometry of the vertical interconnect for port 1 microstrip-to-stripline connection, and (b) PCB cross-section ($d_{via} = 0.15$), and (c) simulated interconnect RL and insertion loss (IL). In (a), the PCB trace connecting the ground vias on L1 is 0.35 mm wide and the signal via-to-ground via center-to-center distance is 0.62 mm. In (b), the L2-L8 dielectric and conductor layer descriptions are those of Fig. 3(c). In (a) and (c), the indices 1 and 2 refer to the interconnects for port 1 and port 2 microstrip-to-stripline connections, respectively. For (c), $p_{L1}^{(1)} = 0.57$, $p_{L1}^{(2)} = 0.45$, and for both interconnects, $p_{L3} = 0.37$, $p_{L4} = 0.49$, $o_{L2} = 0.45$, $o_{L6} = 0.52$, $W_{MSL} = 0.13$. Units: millimeters.

the L4 pad-L6 ground capacitance that can also limit RL. The RLs and ILs of both interconnects are better than 16.1 dB and 0.5 dB, respectively, as can be seen in Fig. 5(c).

Then, the PEC boundary condition of the initial UC without interconnects is eliminated and the interconnects are integrated with the initial UC. Because the feeding now uses a microstrip line that lacks a backing ground plane, an additional Floquet port terminates the space below the UC. The topic of interconnect integration for this class of TL PAAs operating in the K-/Ka-bands is addressed in our work in [40]. Nevertheless, in the V-band, the vertical interconnect parasitic reactances combined with the modification of the UC fields from the interconnect-radiator co-location have a substantial effect on UC scan bandwidth. For this reason, the UC dimensions are adjusted. The UC active VSWR for the adjusted dimensions is shown in Fig. 6. In the principal planes, AVSWR < 2.5 over all the examined bandwidth for $\theta_s = 50°$. However, as shown in Fig. 6(b), AVSWR < 3 over 47.2–50.55 GHz for increased $\theta_s = 60°$. The AVSWR deterioration affecting the upper part of the frequency band is due to E-plane surface wave excitation in the patch substrate [41].

To examine the radiation properties of the UC, we have calculated realized gain in the infinite array environment as in [39], with the results shown in Fig. 7. Up to 50.55 GHz, the difference between the theoretically achievable [42] broadside realized gain and achieved realized gain for $\theta_s \leq 60°$ is below

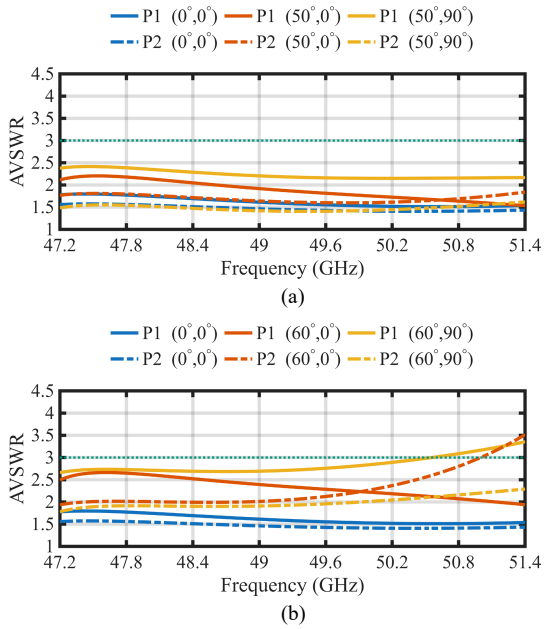

Fig. 6. Simulated port 1 and port 2 AVSWR of the UC with interconnects and adjusted dimensions for (θ_s, ϕ_s) scan angle in a 2-D infinite array. The dotted line marks the AVSWR $= 3$ requirement. (a) Broadside and $\theta_s = 50°$, and (b) broadside and $\theta_s = 60°$. The adjusted dimensions of the UC are: $L_{st}^{(1)} = 0.65$, $W_{sl}^{(1)} = 0.1$, $p_{L1}^{(1)} = 0.53$, $R_p = 0.85$. Units: millimeters. The other dimensions of the UC and interconnects mentioned in Fig. 3 and Fig. 5 remain unchanged.

6 dB. However, at 51.4 GHz, the UC experiences realized gain reduction for wide-angle scanning in the E-plane, with the $|\theta_s| \leq 60°$ realized gain drop relative to the theoretical broadside maximum increasing to approximately 7 dB. This truncation is consistent with the AVSWR findings of Fig. 6.

III. Conclusion

In this work, we presented a PCB-realizable dual-polarized triangular-lattice unit cell (UC) for LEO SATCOM user terminals operating in the V-band. The separately designed phased array antenna UC and vertical interconnects were co-located and their dimensions adjusted, with the resulting UC achieving a 6.85% bandwidth (47.2–50.55 GHz) for active VSWR < 3 and a realized gain drop of less than 6 dB relative to the theoretical maximum for broadside scan. These results demonstrate that the triangular lattice topology commonly employed for K- and Ka-band dual-polarized phased arrays is equally applicable to V-band SATCOM phased arrays, with the enlarged UC area for the same grating-lobe-free scan volume easing future antenna-BFIC integration.

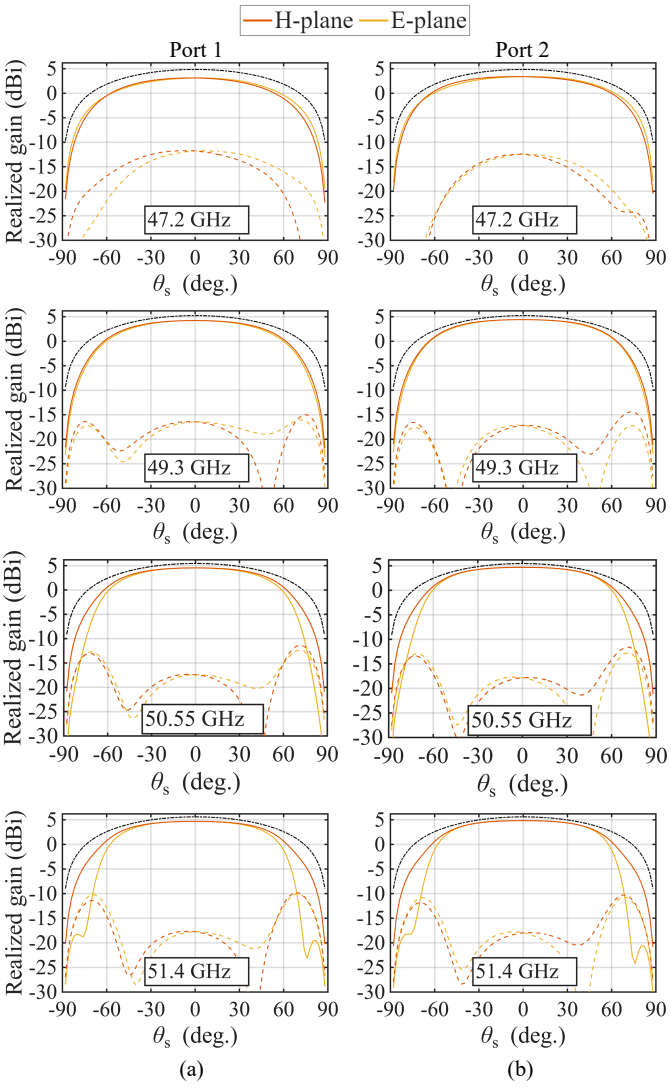

Fig. 7. Realized gain of the UC with interconnects and adjusted dimensions in a 2-D infinite array environment, for E- and H-plane scanning of (a) port 1 and (b) port 2. Solid lines and dashed lines correspond to co- and cross-polarization, respectively.

References

[1] X. Lin, S. Cioni, G. Charbit, N. Chuberre, S. Hellsten, and J.-F. Boutillon, "On the path to 6G: Embracing the next wave of low earth orbit satellite access," *IEEE Communications Magazine*, vol. 59, no. 12, pp. 36–42, 2021.

[2] G. Amendola, D. Cavallo, T. Chaloun, N. Defrance, G. Goussetis, M. Margalef-Rovira, E. Martini, O. Quevedo-Teruel, V. Valenta, N. J. Fonseca, and M. Ettorre, "Low-earth orbit user segment in the Ku and Ka-band: An overview of antennas and RF front-end technologies," *IEEE Microwave Magazine*, vol. 24, no. 2, pp. 32–48, 2023.

[3] D. Zhao, W. Gao, K. Li, H. Wan, Q. Tian, Y. Yi, J. Zhang, and H. Liu, "Q/V-band CMOS beamforming ICs and integrated phased-array antennas," *IEEE Transactions on Circuits and Systems I: Regular Papers*, vol. 72, no. 2, pp. 776–789, 2025.

[4] T.-C. Tsai and A. c. Ulusoy, "A V-band power amplifier in 22-nm FD-SOI supporting instantaneous broadband data transmission at 20 Gb/s," in *2025 16th German Microwave Conference (GeMiC)*, 2025, pp. 459–462.

[5] H. Lee, I. Han, and I. Ju, "Design of a compact, highly efficient, and high-power Q-/V-band SiGe HBT cascode power amplifier with a four-way wilkinson power combiner balun," *IEEE Journal of Solid-State Circuits*, vol. 60, no. 5, pp. 1594–1606, 2025.

[6] I. Han, H. Lee, S.-M. Moon, and I. Ju, "A dual power mode Q/V-band SiGe HBT cascode power amplifier with a novel reconfigurable four-way wilkinson power combiner balun," *IEEE Transactions on Circuits and Systems II: Express Briefs*, vol. 72, no. 1, pp. 168–172, 2025.

[7] S. Shams, A. M. Mahfouz, M. Elsaadany, M. A. M. Hassan, G. Gagnon, and A. A. Kishk, "Circularly polarized V-band orthomode transducer," *IEEE Antennas and Wireless Propagation Letters*, vol. 22, no. 1, pp. 29–33, 2023.

[8] N. Kosugi, S. Higashibata, T. Machida, T. Munehiro, Y. Mori, and

T. Stewart, "Extended V-band helix TWT for future high throughput satellite uplink applications," in *2024 Joint International Vacuum Electronics Conference and International Vacuum Electron Sources Conference (IVEC + IVESC)*, 2024, pp. 1–2.

[9] T.-K. Pham, T. Pham, and R. Sauleau, "Tri-band shared-aperture transmitarray at K-, Ka- and V-bands," in *2024 IEEE Conference on Antenna Measurements and Applications (CAMA)*, 2024, pp. 1–3.

[10] K. van Hastenberg, G. Theis, M. H. Mazaheri, W. M. Abdel-Wahab, A. Smolders, and U. Johannsen, "A polarisation-agile phased-array antenna for satellite and beyond-5G communications," in *2022 IEEE Int. Symp. Antennas Propag. and USNC-URSI Radio Sci. Meeting*, 2022, pp. 1832–1833.

[11] N. Suematsu, T. Furuichi, and S. Tsukamoto, "Q/V-band distributed scalable DBF antenna with direct digital transceiver for LEO constellation satellites," in *2025 IEEE Space Hardware and Radio Conference (SHaRC)*, 2025, pp. 5–7.

[12] W. Gerezgiher, K. Furuuchi, T. Furuichi, S. Tsukamoto, and N. Suematsu, "A tile type V-band 4-element circular polarized patch array antenna with matching circuit," in *2025 International Symposium on Antennas and Propagation (ISAP)*, 2025, pp. 1–2.

[13] P. Gorski, F. Bongard, D. L. del Rio, A. D. Bolado, M. Elsbury, M. Renard, J. Sarmiento, and M. C. Vigano, "Low-cost phased array for land mobile application," in *2025 55th European Microwave Conference (EuMC)*, 2025, pp. 1223–1226.

[14] J.-W. Kim, S.-C. Chae, H.-W. Jo, T.-D. Yeo, and J.-W. Yu, "Wideband circularly polarized phased array antenna system for wide axial ratio scanning," *IEEE Transactions on Antennas and Propagation*, vol. 70, no. 2, pp. 1523–1528, 2022.

[15] G. Gültepe and G. M. Rebeiz, "A 256-element dual-beam dual-polarization Ku-band phased-array with 5 dB/K G/T for simultaneous multi-satellite reception," in *2021 IEEE MTT-S International Microwave Symposium (IMS)*, 2021, pp. 629–631.

[16] T. Takahashi, H. Watanabe, Y. Matsuda, K. Takanishi, A. Hirai, K. Yamamoto, T. Okura, and H. Tsuji, "Dual-beam and wide-angle steering AESA with antenna size scalability for Ka-band SATCOM," in *2024 IEEE International Symposium on Phased Array Systems and Technology (ARRAY)*, 2024, pp. 1–5.

[17] C. Dagnaw, C. Menudier, and M. Thevenot, "Wide angle scanning phased array antenna for Kaband applications," in *2025 55th European Microwave Conference (EuMC)*, 2025, pp. 652–655.

[18] U. Kodak, B. Rupakula, S. Zihir, and G. M. Rebeiz, "60-GHz 64- and 256-element dual-polarized dual-beam wafer-scale phased-array transceivers with reticle-to-reticle stitching," *IEEE Transactions on Microwave Theory and Techniques*, vol. 68, no. 7, pp. 2745–2767, 2020.

[19] E. Shepeleva, A. Vilenskiy, G. Evtyushkin, and A. Lukyanov, "Sub-THz U-slot coupled stacked-patch radiating elements for dual-polarized MIMO array antennas," in *2024 18th Eur. Conf. Antennas Propag.*, pp. 1–5.

[20] T. Liang, S. Wang, A. Alhamed, and G. M. Rebeiz, "Single- and dual-polarized 22–46 GHz multiband phased arrays for 5G MIMO," *IEEE Transactions on Antennas and Propagation*, vol. 73, no. 9, pp. 6263–6275, 2025.

[21] E. Sharp, "A triangular arrangement of planar-array elements that reduces the number needed," *IRE Transactions on Antennas and Propagation*, vol. 9, no. 2, pp. 126–129, 1961.

[22] A. K. Bhattacharyya, "Introduction to Floquet modes in infinite arrays," in *Phased Array Antennas: Floquet Analysis, Synthesis, BFNs, and Active Array Systems*. Hoboken, NJ, USA: Wiley, 2005, ch. 2, pp. 61–87.

[23] S. Harms, M. De Kok, S. Monni, A. Garufo, J.-P. Fraysse, T. Girard, and U. Johannsen, "Waveguide antenna array element with minimized power amplifier load pull for LEO NTNs," in *2024 54th European Microwave Conference (EuMC)*, 2024, pp. 272–275.

[24] L. Polo-López, L. Berretti, E. Menargues, S. Capdevila, G. Toso, and M. García-Vigueras, "Dual-polarized spaceborne phased arrays using tri-ridge evanescent waveguide antennas," *IEEE Antennas and Wireless Propagation Letters*, vol. 24, no. 3, pp. 656–660, 2025.

[25] C. Pfeiffer, J. Massman, and T. Steffen, "3-D printed metallic dual-polarized Vivaldi arrays on square and triangular lattices," *IEEE Transactions on Antennas and Propagation*, vol. 69, no. 12, pp. 8325–8334, 2021.

[26] R. W. Kindt and B. T. Binder, "Wideband planar printed aperture on a triangular lattice for millimeter wave applications," in *2023 17th European Conference on Antennas and Propagation (EuCAP)*, 2023, pp. 1–3.

[27] E. Menargues, S. Capdevila, M. Vizcarro, M. Billod, I. Bengocchea, and M. García-Vigueras, "Metal 3D-printed high-performance radiating panel for SATCOM AESA terminals," in *2024 IEEE International Symposium on Phased Array Systems and Technology (ARRAY)*, 2024, pp. 1–5.

[28] H. Kähkönen, J. Ala-Laurinaho, and V. Viikari, "Dual-polarized Ka-band Vivaldi antenna array," *IEEE Transactions on Antennas and Propagation*, vol. 68, no. 4, pp. 2675–2683, 2020.

[29] S. Hernandez-Rodriguez, C. Dagnaw, M. Thevenot, C. Hallepée, and C. Menudier, "A co-simulation methodology for the optimization of active phased arrays," in *2025 IEEE Conference on Antenna Measurements and Applications (CAMA)*, 2025, pp. 1–5.

[30] Y. Zhang, A. R. Vilenskiy, and M. V. Ivashina, "Wideband open-ended ridge gap waveguide antenna elements for 1-D and 2-D wide-angle scanning phased arrays at 100 GHz," *IEEE Antennas and Wireless Propagation Letters*, vol. 21, no. 5, pp. 883–887, 2022.

[31] F. Xie, Z.-C. Hao, Z. Li, J.-Y. Zhang, Z.-J. Guo, C.-Y. Ding, Z.-W. Miao, J. Chen, Z. Jiang, and W. Hong, "A 220-GHz planar triangular lattice transmitter array with 42.7-dBm peak EIRP for long-distance high-data-rate wireless communication," *IEEE Transactions on Microwave Theory and Techniques*, vol. 73, no. 6, pp. 3194–3208, 2025.

[32] Q. Zhang, X. Cheng, Y. Yao, and J. Yu, "A 60 GHz wide-angle scanning planar phased array antenna in triangular lattice," in *2023 IEEE MTT-S International Wireless Symposium (IWS)*, 2023, pp. 1–3.

[33] A. Gonzalez, E. A. Alwan, and J. L. Volakis, "Phased array with 45° scanning and over 65dB polarization purity from 53–100GHz using PCB flip-chip technology," in *2020 IEEE MTT-S Latin America Microwave Conference (LAMC 2020)*, 2021, pp. 1–4.

[34] S. M. Moghaddam, J. Yang, and A. U. Zaman, "Fully-planar ultrawideband tightly-coupled array (FPU-TCA) with integrated feed for wide-scanning millimeter-wave applications," *IEEE Transactions on Antennas and Propagation*, vol. 68, no. 9, pp. 6591–6601, 2020.

[35] P. Dufilie, E. Kowalski, M. D. Conway, D. Du Russel, and A. J. Fenn, "V-band stacked patch antenna phased array," in *2022 IEEE International Symposium on Phased Array Systems & Technology (PAST)*, 2022, pp. 01–07.

[36] M. Hamza, C. Exadaktylos, C. L. Zekios, and S. V. Georgakopoulos, "An ultrawideband fully planar inverted-L element (FILE) array," *IEEE Transactions on Antennas and Propagation*, vol. 73, no. 1, pp. 174–187, 2025.

[37] Y. Zhu, A. R. Vilenskiy, O. A. Iupikov, P. S. Krasov, T. Emanuelsson, G. Lasser, and M. V. Ivashina, "Millimeter-wave reconfigurable intelligent surface with independent and continuous amplitude-phase control: Unit cell design and circuit model," *IEEE Transactions on Antennas and Propagation*, vol. 73, no. 10, pp. 7627–7641, 2025.

[38] J. Fan, A. Hardock, R. Rimolo-Donadio, S. Müller, Y. H. Kwark, and C. Schuster, "Signal integrity: Efficient, physics-based via modeling: Return path, impedance, and stub effect control," *IEEE Electromagnetic Compatibility Magazine*, vol. 3, no. 1, pp. 76–84, 2014.

[39] T. Chaloun, P. Grüner, and W. Menzel, "Design and analysis of a novel wide-angle scanning stub-loaded cavity array element," *IEEE Open Journal of Antennas and Propagation*, vol. 3, pp. 783–797, 2022.

[40] T. Pavlidis, T. Schäfer, A. R. Vilenskiy, L. Nyström, A. A. Kishk, and M. V. Ivashina, "Dual-polarized, K-/Ka-band wide 2-D-scanning patch antenna array on a triangular lattice for SATCOM-on-the-move applications," submitted to IEEE Antennas and Wireless Propagation Letters.

[41] D. Pozar and D. Schaubert, "Scan blindness in infinite phased arrays of printed dipoles," *IEEE Transactions on Antennas and Propagation*, vol. 32, no. 6, pp. 602–610, 1984.

[42] P. Hannan, "The element-gain paradox for a phased-array antenna," *IEEE Transactions on Antennas and Propagation*, vol. 12, no. 4, pp. 423–433, 1964.